

1 **Solar photoelectro-Fenton treatment of a mixture of parabens spiked**
2 **into secondary treated wastewater effluent at low input current**

3 Juliana R. Steter, Enric Brillas, Ignasi Sirés *

4 *Laboratori d'Electroquímica dels Materials i del Medi Ambient, Departament de Química*
5 *Física, Facultat de Química, Universitat de Barcelona, Martí i Franquès 1-11, 08028*
6 *Barcelona, Spain*

7 Paper submitted to be published in *Applied Catalysis B: Environmental*

8 *Corresponding author: Tel.: +34 934039240; fax: +34 934021231.

9 E-mail address: i.sires@ub.edu (I. Sirés)

10

11 **Abstract**

12 Aqueous mixtures of methyl, ethyl and propyl paraben (MeP, EtP and PrP) prepared in real
13 urban wastewater with low conductivity were treated by solar photoelectro-Fenton (SPEF)
14 process at low input current ($j = 10 \text{ mA cm}^{-2}$) using a pre-pilot plant with an electrochemical
15 reactor equipped with an air-diffusion cathode to electrogenerate H_2O_2 and a boron-doped
16 diamond (BDD) or RuO_2 -based anode. Comparative trials in simulated water matrices with or
17 without Cl^- in the absence of natural organic matter (NOM) always led to a slower decay of
18 parabens concentration and total organic carbon (TOC). This was mainly due to the superior
19 regeneration of Fe^{2+} from photoreduction of Fe(III) complexes formed with NOM in real
20 wastewater compared to that from $\text{Fe}(\text{OH})^{2+}$. In all matrices, a catalyst concentration as low
21 as 0.20 mM Fe^{2+} was enough to ensure the production of $\bullet\text{OH}$ in the bulk from Fenton's
22 reaction. SPEF with BDD yielded a complete removal of parabens in 180 min and 66%
23 mineralization at 240 min. This gave rise to the greatest mineralization current efficiencies
24 reported so far, up to 1000%, with a low energy consumption of $84 \text{ kWh (kg TOC)}^{-1}$. The
25 synergy between homogeneous and heterogeneous catalysis, which allowed the efficient
26 dosage of $\bullet\text{OH}$ and $\text{M}(\bullet\text{OH})$ at low j , with simultaneous action of high UV power from
27 sunlight justified such a good performance. Analogous apparent rate constants were
28 determined for MeP, EtP and PrP. Slower decays were found with RuO_2 -based anode due to
29 its lower oxidation power. As a result, the MCE was 425% as maximum, but a lower energy
30 consumption of $52 \text{ kWh (kg TOC)}^{-1}$ was needed. Since the role of active chlorine was of
31 minor importance, the formation of toxic, refractory chloroderivatives was minimized. All by-
32 products were transformed into malic, formic and oxalic acids prior to total mineralization.

33 *Keywords:* Boron-doped diamond; Dimensionally stable anode; Parabens; Solar photoelectro-
34 Fenton; Wastewater treatment

35 **1. Introduction**

36 In recent years, the electrochemical technologies for the removal of man-made organic
37 contaminants from water bodies have seen an extraordinary development, in parallel to the
38 progressively greater environmental and health concerns associated to xenobiotics. In
39 particular, major interest is focused on two kinds of electrochemical advanced oxidation
40 processes (EAOPs) that allow, in many cases, the total transformation of the parent pollutants
41 into innocuous by-products: electro-oxidation (EO) and Fenton-based EAOPs like electro-
42 Fenton (EF) and UVA or solar photoelectro-Fenton (PEF and SPEF) [1].

43 EO is the simplest EAOP for treating organic pollutants, since it relies on the promotion
44 of heterogeneous catalysis at the surface of a suitable anode (M), yielding adsorbed hydroxyl
45 radicals ($\bullet\text{OH}$) from water oxidation as follows:



47 Boron-doped diamond (BDD) exhibits the highest performance in EO owing to its large
48 overpotential for O_2 evolution [2], but it presents some shortcomings like high cost, electrode
49 instability during wastewater treatment and difficulties to fabricate large electrodes [3]. This
50 has led to the alternative use of metal oxides as dimensionally stable anodes, which allow the
51 removal of recalcitrant chemicals at a much lower cost [4]. However, the relationship between
52 the surface structure of metal oxides and their electrocatalytic ability is not so clear as in the
53 case of BDD and hence, results tend to be case-sensitive. In contrast to non-active BDD
54 anode, it has been established that the radical $\text{M}(\bullet\text{OH})$ formed from Reaction (1) on the
55 surface of active metal oxides is partially transformed into the weaker oxidant MO , thus
56 conferring to the anode a lower oxidation ability. But, in some cases, the enhanced adsorption
57 of organics on the surface of metal oxides can improve the degradation process [1].

58 Low amounts of less powerful oxidants like O_3 and $S_2O_8^{2-}$ may be formed in
59 concomitance with $M(\bullet OH)$. Some authors have combined conventional EO with cathodic
60 electrogeneration of H_2O_2 from two-electron reduction of O_2 according to Reaction (2), giving
61 rise to the EO- H_2O_2 process [1]:



63 The effectiveness of EO- H_2O_2 can be substantially enhanced upon homogeneous
64 catalysis with metal cations like Fe^{2+} at pH \sim 3.0 [5]. In EF, H_2O_2 formed via Reaction (2)
65 reacts with added Fe^{2+} according to Fenton's Reaction (3). Further enhancement is reached in
66 PEF or SPEF under UVA irradiation, which maintains the catalytic cycle by promoting the
67 continuous photolytic reduction of Fe(III) species via photo-Fenton Reaction (4).



70 Carbon-based cathodes are optimum to carry out EF, PEF and SPEF because they allow
71 the efficient production of H_2O_2 at a low cost and toxicity. Among them, carbon felt [6-10]
72 and air-diffusion electrodes [11-17] have been widely explored, being reticulated vitreous
73 carbon [18,19] and BDD [20] more rarely employed.

74 At present, SPEF with air-diffusion cathode is the best option to mineralize organic
75 pollutants at acidic pH, which can be explained by the large amount of H_2O_2 formed from
76 Reaction (2) and the high UV power of sunlight compared to commercial UVA lamps [21-
77 29]. The effectiveness of SPEF has been demonstrated by treating model organic pollutants
78 such as pesticides [21], dyes [22-25], pharmaceuticals [26,27] and phytochemicals [28], as
79 well as real landfill leachate [29]. In all these cases, the high conductivity of treated solutions
80 favored the application of high current densities ($> 33 \text{ mA cm}^{-2}$), thus accelerating the
81 degradation to the detriment of current efficiency. However, the performance of SPEF in real

82 water matrices with low conductivity has not been reported yet. Furthermore, such samples
83 usually contain Cl^- , which is plausibly oxidized to active chlorine (Cl_2 , HClO and/or ClO^-)
84 that competes with $\text{M}(\bullet\text{OH})$ and $\bullet\text{OH}$ formed at the anode and in the bulk, respectively [30-
85 32].

86 Nowadays, parabens are organic pollutants of major concern because they act as
87 endocrine disruptors [33] and may cause human cancers and dermatitis [34,35]. They are
88 ubiquitous in our daily lives since they are widely used as antimicrobial preservatives in
89 processed food, medicines, cosmetics and toiletries [36,37], despite the increasing restrictions
90 worldwide. As a result of their widespread use along with their facile dispersion and
91 bioaccumulation in the environment [38], the occurrence in effluents of municipal wastewater
92 treatment facilities (WWTFs) has been documented [39], thus being necessary to develop
93 more effective and efficient water reclamation technologies. Advanced treatment of parabens
94 in water with mediation of hydroxyl radicals produced on site has been performed by O_3 -
95 based methods [40], Fenton process [41,42], and UVA or solar photocatalysis with TiO_2
96 [43,44]. A more efficient degradation has been reported by EAOPs like EO with BDD anode
97 [45-47], as well as EF or PEF with UVA light [48]. These previous studies were focused on
98 methyl paraben (MeP) in high conductivity media using high current densities.

99 This article presents the degradation of a mixture of three parabens, namely methyl (MeP),
100 ethyl (EtP) and propyl (PrP) paraben dissolved in urban wastewater with low conductivity (~
101 3 mS cm^{-1}). Solutions of 2.5 L have been treated in batch mode, employing a pre-pilot plant
102 including a photoreactor and an undivided filter-press cell equipped with a BDD or RuO_2 -
103 based anode and an air-diffusion cathode. Most of the experiments have been performed
104 under SPEF conditions at low current density (j) of 10 mA cm^{-2} . The effect of j and parabens
105 and iron concentration has also been assessed. For comparison, EO, EF and SPEF trials in
106 synthetic solutions prepared with Milli-Q water have been made as well. The performance of

107 each treatment has been interpreted from TOC abatement, parabens decay, current efficiency
108 profiles and energy consumption. The main primary reaction by-products and final aliphatic
109 carboxylic acids have been identified by chromatographic techniques.

110 **2. Materials and methods**

111 *2.1. Chemicals*

112 MeP, EtP and PrP with $\geq 99\%$ purity were supplied by Sigma-Aldrich. Anhydrous
113 sodium sulfate used as supporting electrolyte and iron(II) sulfate heptahydrate used as catalyst
114 in EF and SPEF were of analytical grade from Fluka. Analytical grade sulfuric acid from
115 Merck was used to adjust the solution pH to 3.0. All other chemicals were of high
116 performance liquid chromatography (HPLC) or analytical grade from Panreac and Sigma-
117 Aldrich. Synthetic solutions were prepared with ultrapure water from a Millipore Milli-Q
118 system.

119 *2.2. Aqueous media*

120 Parabens to be degraded were spiked into three different water matrices:

121 (i) A solution with 5 mM Na_2SO_4 in deionized water, with conductivity of 1.70 mS cm^{-1} .

122 (ii) A simulated water matrix (SWM) prepared with deionized water and containing the
123 main ions that are typically found in WWTFs (Na^+ , NH_4^+ , SO_4^{2-} , Cl^- , NO_2^- and NO_3^-), but in
124 the absence of natural organic matter, yielding a conductivity of 1.75 mS cm^{-1} .

125 (iii) Real wastewater (RWW) obtained from the secondary decanter of a municipal
126 WWTF near Barcelona. The sample, which was kept at 4°C all the time before use, contained
127 81.1 mg L^{-1} of total carbon and 10.8 mg L^{-1} of total organic carbon (TOC), its pH was 8.1 and
128 its conductivity was 2.20 mS cm^{-1} . Cations included $0.20 \text{ mg L}^{-1} \text{ Fe}^{2+}$, $33.6 \text{ mg L}^{-1} \text{ K}^+$, 211.7
129 $\text{mg L}^{-1} \text{ Na}^+$ and $36.9 \text{ mg L}^{-1} \text{ NH}_4^+$, apart from traces of Ca^{2+} and Mg^{2+} . Anions included 0.79
130 $\text{mg L}^{-1} \text{ NO}_2^-$, $0.85 \text{ mg L}^{-1} \text{ NO}_3^-$, $318.0 \text{ mg L}^{-1} \text{ Cl}^-$ and $141.3 \text{ mg L}^{-1} \text{ SO}_4^{2-}$.

131 Upon pH adjustment to 3.0, the final conductivity slightly increased up to 1.75, 1.80 and
132 3.70 mS cm⁻¹, respectively. Almost all the electrolyses were made with mixtures of 0.30 mM
133 MeP + 0.30 mM EtP + 0.30 mM PrP (initial TOC content of 100 mg L⁻¹).

134 2.3. Bulk electrolyses

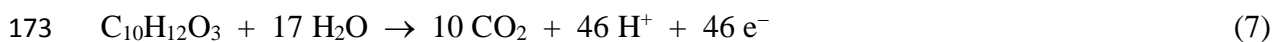
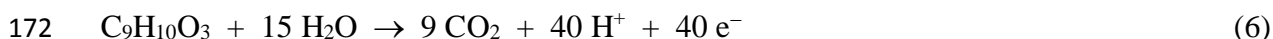
135 A flow plant operating in batch mode was employed to treat solutions of 2.5 L containing
136 equimolar mixtures of the three parabens [23]. The solution, kept into a plastic reservoir, was
137 continuously recirculated at a fixed flow rate of 180 L h⁻¹ using a centrifugal pump, and
138 maintaining a constant temperature of 30 °C by means of two heat exchangers. The solution
139 entered into a filter-press electrochemical cell equipped with a 20 cm² BDD anode from
140 NeoCoat or RuO₂-based plate from NMT Electrodes, along with a 20 cm² carbon-PTFE air-
141 diffusion cathode from E-TEK, with an interelectrode gap of 1.2 cm. The cathode was
142 prepared by painting a carbon cloth with the wet paste resulting from an equimass mixture of
143 Vulcan XC-72 conductive specialty carbon black and 30-N PTFE dispersion in water,
144 followed by compression at 350 °C for 30 min. The dry face of the cathode was fed with air
145 through a gas chamber at an overpressure of about 8.6 kPa regulated with a back-pressure
146 gauge, thus ensuring the continuous H₂O₂ production at the wet face from O₂ reduction on the
147 carbon catalyst. The dry face of the cathode was fed with air through a gas chamber at an
148 overpressure of about 8.6 kPa regulated with a back-pressure gauge, thus ensuring a
149 continuous H₂O₂ production at the wet face. The cell outlet was connected to a planar solar
150 photoreactor of 600 mL capacity for the SPEF trials, which was covered with an opaque cloth
151 in the EO-H₂O₂ and EF trials. A constant current was supplied by an Agilent 6552A DC
152 power source, which displayed the cell voltage (E_{cell}) as well. The photoreactor was tilted 41°
153 (latitude of facilities in Barcelona) to collect most of the direct sun rays. SPEF assays were
154 carried out in sunny days during the summer of 2016 and the natural UV irradiance (300-400
155 nm) was about 30-35 W m⁻², as determined with a Kipp&Zonen CUV 5 radiometer. The

156 assays were typically carried out for 240 min, since longer electrolyses entailed a remarkable
157 decrease of irradiance.

158 2.4. Instruments and analytical methods

159 The conductivity in each medium was determined from the electrical conductance
160 measured on a Metrohm 644 conductometer, whereas the solution pH was measured on a
161 Crison GLP 22 pH-meter. For all subsequent analyses, samples were filtered using 0.45 μm
162 PTFE syringe filters from Whatman. The H_2O_2 and active chlorine contents accumulated from
163 *in situ* electrogeneration were determined from the absorbance values obtained at $\lambda = 408$ and
164 515 nm, respectively, employing a Shimadzu 1800 UV/Vis spectrophotometer at 25 $^\circ\text{C}$
165 according to the Ti(IV) complexation and *N,N*-diethyl-*p*-phenylenediamine colorimetric
166 methods [49,50]. The NH_4^+ content was evaluated through the indophenol blue method using
167 the same spectrophotometer. The concentration of all other cations as well as that of anions in
168 the RWW sample was determined by ion chromatography as previously reported [51].

169 TOC values were obtained from direct injection into a VCSN TOC analyzer from
170 Shimadzu. Assuming the following reactions for total mineralization of MeP, EtP and PrP:



174 and considering that equimolar mixtures were always prepared, the average number of
175 electrons was $n = 40$, whereas the average number of C atoms was $m = 9$. Hence, the
176 mineralization current efficiency (MCE) for each trial was estimated as follows [21]:

$$177 \% \text{MCE} = \frac{nFV_s \Delta(\text{TOC})_{\text{exp}}}{4.32 \times 10^7 \text{ mIt}} \times 100 \quad (8)$$

178 where F is the Faraday constant ($96,485 \text{ C mol}^{-1}$), V_s is the solution volume (L), $\Delta(\text{TOC})_{\text{exp}}$ is
179 the experimental TOC decay (mg C L^{-1}), 4.32×10^7 is a conversion factor to homogenize the
180 units, I is the applied current (A) and t is the electrolysis time (h).

181 The specific energy consumption per unit TOC mass (EC_{TOC}) was estimated as follows
182 [21]:

$$183 \text{EC}_{\text{TOC}} (\text{kWh (kg TOC)}^{-1}) = \frac{1000 E_{\text{cell}} I t}{V_s \Delta(\text{TOC})_{\text{exp}}} \quad (9)$$

184 where E_{cell} is in V and the rest of parameters has been already defined. The average E_{cell} value
185 in each system is given in Table S1 of Supplementary Material.

186 The concentration decay of MeP, EtP and PrP was assessed by reversed-phase HPLC on
187 a Waters 600 LC fitted with a BDS Hypersil C18 $6 \mu\text{m}$, $250 \text{ mm} \times 4.6 \text{ mm}$, column at $35 \text{ }^\circ\text{C}$
188 and coupled to a Waters 996 PDA detector set at each maximum wavelength in the UV
189 region. Most of the samples were conveniently diluted with acetonitrile and/or mixed with
190 sodium thiosulfate to prevent further degradation once withdrawn upon electrolysis. A 40:60
191 (v/v) acetonitrile/water mixture was eluted at 1 mL min^{-1} as mobile phase, yielding perfectly
192 symmetric peaks at 5.2, 7.1 and 10.7 min. related to MeP, EtP and PrP, respectively. Linear
193 carboxylic acids were identified by ion-exclusion HPLC using the same chromatograph fitted
194 with a Bio-Rad Aminex HPX 87H, $300 \text{ mm} \times 7.8 \text{ mm}$, column at $35 \text{ }^\circ\text{C}$, and setting the
195 detector at $\lambda = 210 \text{ nm}$. A $4 \text{ mM H}_2\text{SO}_4$ solution was eluted at 0.6 mL min^{-1} as mobile phase,
196 yielding peaks at 6.7, 9.6 and 13.9 min for oxalic, malic and formic acid, respectively.

197 The main primary aromatic by-products formed in the absence and presence of Cl^- were
198 identified by treating mixtures of the three parabens (0.30 mM each) in either $5 \text{ mM Na}_2\text{SO}_4$
199 or RWW by SPEF for 10, 30, 60 and 240 min. The organic components contained in 50 mL
200 of electrolyzed samples were concentrated using solid-phase extraction tips (Agilent Bond
201 Elute OMIX SPE), followed by elution with 2 mL of methanol. After concentration down to 1
202 mL with a gentle N_2 stream, the final samples were analyzed by gas chromatography-mass

203 spectrometry (GC-MS). An Agilent Technologies system composed of a 6890N
204 chromatograph coupled to a 5975 XL mass spectrometer, operating in electron ionization
205 mode at 70 eV, was employed. A non-polar Teknokroma Sapiens-X5.ms 0.25 μm , 30 m \times
206 0.25 mm, column was used, with the following temperature ramp: 36 $^{\circ}\text{C}$ for 1 min, 5 $^{\circ}\text{C min}^{-1}$
207 up to 320 $^{\circ}\text{C}$ and hold time 10 min. The temperature of the inlet, source and transfer line was
208 250, 230 and 280 $^{\circ}\text{C}$. A NIST05 MS library allowed the identification of the mass spectra.

209 **3. Results and discussion**

210 *3.1. Treatment of mixtures of parabens in Na_2SO_4 using a BDD/air-diffusion cell*

211 As a preliminary investigation, the performance of various EAOPs was assessed in a
212 synthetic aqueous matrix containing Na_2SO_4 as single electrolyte. This kind of study has been
213 usually made in acidic solutions with high conductivity (i.e., 0.050 M Na_2SO_4) [21,24], but in
214 the present work the electrolyses were carried out in a 5 mM Na_2SO_4 solution at pH 3.0
215 aiming to mimic the low conductivity of real effluents from WWTFs ($\sim 3.70 \text{ mS cm}^{-1}$ after
216 pH adjustment). A pre-pilot plant with a BDD/air-diffusion cell was employed to treat
217 solutions of 2.5 L at a j as low as 10 mA cm^{-2} due to the low conductivity.

218 The ability of the flow cell to electrogenerate H_2O_2 under different conditions is depicted
219 in Fig. S1 of Supplementary Material. In the absence of Fe^{2+} in the dark (EO- H_2O_2
220 conditions), a continuous accumulation of H_2O_2 from Reaction (2) was observed, attaining 4.2
221 mM at 240 min. The accumulation rate diminished over time, as a result of the progressively
222 larger destruction of H_2O_2 by oxidation at the BDD surface. Worth mentioning, the
223 electrogeneration at such low j was more efficient than that reported elsewhere at high j ; for
224 example, 8.0 mM H_2O_2 was accumulated at 240 min in 0.050 M HClO_4 at 50 mA cm^{-2} [31].
225 This means that at low j , parasitic reactions like reduction of H_2O_2 to H_2O and H^+ to H_2 are
226 minimized. A much lower steady H_2O_2 concentration of $\sim 2.4 \text{ mM}$ was reached from 60 min

227 working in the presence of 0.20 mM Fe²⁺ (EF conditions), once the H₂O₂ production was
228 perfectly counterbalanced by its destruction at the anode surface and in the bulk. In general,
229 0.5-1.0 mM Fe²⁺ is added to promote Fenton's Reaction (3) in systems with an air-diffusion
230 cathode [1], but a lower catalyst concentration seems enough at low *j*. This is interesting
231 aiming to further propose the treatment of RWW, where the addition of iron must be limited
232 from an economic and environmental standpoint. Finally, an analogous electrolysis but under
233 solar irradiation (SPEF conditions) yielded a lower accumulation of 1.4 mM H₂O₂ at 240 min.
234 This is explained by the continuous photoreduction of Fe(III), produced via Fenton's Reaction
235 (3), to Fe²⁺ from Reaction (4), accelerating the destruction of H₂O₂ in the bulk. As a result, the
236 *in situ* production of •OH in the bulk at low *j* was enhanced in the order EO-H₂O₂ < EF <
237 SPEF.

238 Next, the ability of the three EAOPs to degrade equimolar mixtures of three parabens
239 (0.30 mM each) in 5 mM Na₂SO₄ at pH 3.0 was compared. Fig. S2a, c and e of
240 Supplementary Material shows the concentration decay of MeP, EtP and PrP with electrolysis
241 time. In EO-H₂O₂ (Fig. S2a), about 65% of parabens removal was achieved at 360 min upon
242 reaction with BDD(•OH) formed in the anode vicinity from Reaction (1). No substantial
243 difference could be appreciated between the three profiles. However, the corresponding
244 pseudo-first-order kinetic analysis of Fig. S2b highlights a slightly higher slope for PrP
245 compared to MeP and EtP. This is more evident from the apparent rate constants summarized
246 in Table 1, showing that $k_{\text{PrP}} = 3.1 \times 10^{-3} \text{ min}^{-1} > k_{\text{MeP}} \sim k_{\text{EtP}} \sim 2.6 \times 10^{-3} \text{ min}^{-1}$, which suggests
247 the occurrence of a larger adsorption of PrP on BDD. A much quicker decay, with total
248 disappearance of all parabens at 360 min despite the low *j*, was found in EF with 0.20 mM
249 Fe²⁺, as can be seen in Fig. S2c. In this process, no difference could be observed between the
250 three degradation profiles, meaning that •OH formed in the bulk was the main oxidant. The
251 corresponding kinetic analysis presented in Fig. S2d yielded the rate constants included in

252 Table 1, with a mean value of 0.013 min^{-1} . A dramatic acceleration of the parabens
253 degradation was achieved in SPEF with 0.20 mM Fe^{2+} . As shown in Fig. S2e, only 180 min
254 were required to completely remove MeP, EtP and PrP, which is confirmed by the much
255 greater mean rate constant of 0.020 min^{-1} (see Fig. S2f and Table 1). The outstanding
256 contribution of continuous Fe^{2+} regeneration and additional $\bullet\text{OH}$ production from photo-
257 Fenton Reaction (4) upon sunlight irradiation is confirmed, eventually enhancing the $\bullet\text{OH}$
258 production from Fenton's Reaction (3).

259 TOC abatement for the same three trials is illustrated in Fig. S3 of Supplementary
260 Material. In EO- H_2O_2 , 35% mineralization was attained after 240 min. Since a low amount of
261 BDD($\bullet\text{OH}$), the only oxidant in this process, was produced at 10 mA cm^{-2} , the gradual
262 degradation of reaction by-products occurred very slowly. In fact, note that 50% of the initial
263 parabens content was still present in solution (Fig. S2a). A very similar TOC decay was
264 achieved in EF, ending in a close TOC value at 240 min. This means that $\bullet\text{OH}$ produced from
265 Fenton's Reaction (3) can easily oxidize the parent pollutants (Fig. S2c), but not the very
266 refractory complexes formed between Fe(III) and organic intermediates like linear carboxylic
267 acids. Such complexes can be typically degraded by BDD($\bullet\text{OH}$), but its concentration was too
268 small at low j , as mentioned before. A substantially larger mineralization of 51% was attained
269 in SPEF. This may be explained by the crucial role of high power UV light from natural
270 sunlight, which promoted: (i) the production of larger quantities of $\bullet\text{OH}$, induced by photo-
271 Fenton Reaction (4), as mentioned above (Fig. S2e), and (ii) the more decisive
272 photodecarboxylation of refractory Fe(III)-carboxylate complexes as follows [1]:



274 Therefore, sunlight irradiation ensured the progressive TOC decay despite the low input
275 current. Fig. S4 of Supplementary Material highlights the kind of aliphatic by-products,

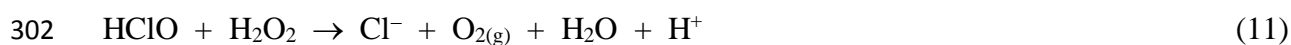
276 mostly present as Fe(III) complexes [1], that were accumulated during the above SPEF
277 degradation of the parabens mixture. Oxalic acid was accumulated at a very small
278 concentration ($< 5 \text{ mg L}^{-1}$) during the whole electrolysis, owing to the very effective
279 photodegradation of the Fe(III)-oxalate complexes [24]. In contrast, a much larger
280 accumulation was found for malic acid, attaining 66 mg L^{-1} as maximal at 120-150 min.
281 Later, the concentration progressively decayed down to 46 mg L^{-1} since it was more quickly
282 destroyed than formed, in agreement with the small amount of remaining parabens (precursors
283 of carboxylic acids) at that time (Fig. S2e). Note that malic acid only accounted for 16 mg L^{-1}
284 TOC at 240 min, which is only a 33% of the solution TOC (Fig. S3), suggesting that other
285 kinds of refractory by-products were also accumulated.

286 *3.2. SPEF treatment in real wastewater matrix using a BDD/air-diffusion cell*

287 Once the degradation ability of the three EAOPs was corroborated at low j in a simple
288 aqueous matrix, the same pre-pilot flow plant and cell were employed to degrade mixtures of
289 the three mentioned parabens (0.30 mM each) in the presence of 0.20 mM Fe^{2+} at pH 3.0 by
290 SPEF at 10 mA cm^{-2} in SWM or RWW. The initial TOC was 100 mg L^{-1} in SMW, whereas it
291 was $\sim 110 \text{ mg L}^{-1}$ in RWW due to the presence of natural organic matter (NOM).

292 Fig. 1 informs about the time course of the concentration of H_2O_2 and active chlorine
293 accumulated along the SPEF treatment in each medium. H_2O_2 was formed via Reaction (2)
294 gradually increasing its content up to a steady value from 120 min. At 240 min, 1.45 and 1.85
295 mM was attained in SWM and RWW, respectively. On the other hand, the final active
296 chlorine concentration arising from Cl^- oxidation at the BDD anode surface was 1.40 and
297 1.55 mg L^{-1} in SWM and RWW, respectively. A higher accumulation of both oxidants was
298 then obtained in RWW, which can be explained by the easier reaction of active chlorine with
299 H_2O_2 according to Reaction (11) in SWM [48], which leads to a smaller steady concentration

300 of both species compared to RWW. In this latter matrix, the oxidation of additional NOM
301 with $\bullet\text{OH}$ and HClO interferes and makes Reaction (11) more difficult.



303 Fig. 2 shows the decay of MeP, EtP and PrP concentration with electrolysis time during
304 the same trials. According to Fig. 2a, total removal of the three parabens in SWM occurred at
305 180 min, presenting almost identical profiles to those in 5 mM Na_2SO_4 (Fig. S2). This was
306 corroborated from the rate constants obtained from the kinetic analysis shown in the inset,
307 yielding an average value of 0.019 min^{-1} (Table 1) that practically coincided with that found
308 in Na_2SO_4 . Hence, it can be concluded that the presence of Cl^- was not beneficial, which is in
309 contrast to findings reported in literature. For example, the formation of active chlorine
310 accelerated the removal of the naproxen by Fenton-based EAOPs [31]. This apparent
311 contradiction can be related to the really small amount of chlorine generated at low j (Fig. 1)
312 and thus, the main reactive species to justify the degradation of parabens in SWM also
313 corresponded to $\bullet\text{OH}$ formed from Fenton's Reaction (3), greatly promoted upon sunlight
314 irradiation. This evidence allows discarding as substantial contribution of a recently suggested
315 Fenton-like Reaction [32,52]:



317 A faster disappearance of MeP, EtP and PrP was achieved in RWW, as can be observed
318 in Fig. 2b, requiring 150 min for total concentration decrease. These decays were quicker than
319 in the other two matrices, being corroborated from the linear fittings of the inset that yielded a
320 rate constant of 0.025 min^{-1} on average (Table 1). This can be explained by: (i) the superior
321 regeneration of Fe^{2+} from photoreduction of Fe(III) complexes formed with natural organic
322 matter compared to that from photo-Fenton Reaction (4), and (ii) the possible formation of
323 reactive species upon photolysis of the RWW matrix. The additional production of $\bullet\text{OH}$ from

324 Reaction (12), plausible considering the higher HClO content compared to that of SWM (Fig.
325 1), was probably much less relevant.

326 Normalized TOC abatement for these trials is depicted in Fig. 3. In SWM, 52%
327 mineralization was reached at 240 min. This percentage as well as the trend are very similar to
328 those obtained in 5 mM Na₂SO₄, confirming the minor role of active chlorine. This is in
329 contrast to typical studies at high j , where the formation of free and complexed chloro-
330 organics causes the deceleration of TOC removal due to their refractoriness to M(\bullet OH) and
331 \bullet OH [53], and can be explained by the very low content of active chlorine formed at low j .
332 The minimization of chloroderivatives is then a very positive outcome from SPEF treatment
333 at low input current. On the other hand, in RWW, up to 66% TOC abatement could be
334 attained at the end of the electrolysis, which is in agreement with the aforementioned superior
335 photoreductive and photolytic effects of sunlight in the presence of NOM. It is worth to
336 mention that, at high j , the presence of such organic matter is rather detrimental [53], because
337 it acts as a radical scavenger consuming M(\bullet OH) and \bullet OH. As a result, it is more quickly
338 destroyed, thus minimizing the formation of photosensitive complexes with Fe(III) that
339 constitute a source of Fe²⁺.

340 To end with the investigation using the BDD/air-diffusion cell, the current efficiency and
341 energy consumption were calculated from Eq. (8) and (9), respectively, since these parameters
342 may be better indicators to show the positive impact of low j in electrochemical treatments.
343 Fig. 4 compares the trends of MCE and EC_{TOC} for the SPEF treatment of mixtures of MeP,
344 EtP and PrP (0.30 mM each) in the three media mentioned above, at $j = 10 \text{ mA cm}^{-2}$. The
345 maximum efficiencies in all matrices were achieved during the early stages, as can be seen in
346 Fig. 4a. MCE values of 380%, 450% and up to 1000% were determined in 5 mM Na₂SO₄,
347 SWM and RWW, respectively. Such impressive MCE has never been reported so far, and can
348 be related to: (i) a very efficient action of \bullet OH at low j generated from Fenton's Reaction (3)

349 upon minimization of parasitic reactions, which was enormously empowered by photolytic
350 Reaction (4), combined with (ii) the great photoreductive and photolytic effect of sunlight on
351 Fe(III) complexes, mainly with those formed with final carboxylic acids that are efficiently
352 and rapidly photodecomposed via Reaction (10). The higher efficiency in RWW and the
353 similarity between trials in SWM and Na₂SO₄ media are in agreement with TOC decays (Fig.
354 S3 and 3). The progressive decay of MCE over time was due to decrease of organic load upon
355 mineralization and the larger refractoriness of by-products, although an MCE as high as 200%
356 MCE was still obtained at 240 min. As expected, the EC_{TOC} trends with electrolysis time
357 presented the opposite behavior, with higher consumption in the order RWW < SWM ~
358 Na₂SO₄. Much lower consumptions compared to previous studies, i.e., 54, 110 and 123 kWh
359 (kg TOC)⁻¹, were required in the above media for 50% TOC reduction, respectively. For
360 example, EC_{TOC} = 2400 kWh (kg TOC)⁻¹ resulted from SPEF treatment of pesticide
361 tebuthiuron in 0.050 M Na₂SO₄ with 0.50 mM Fe²⁺ at pH 3.0 using a BDD/air-diffusion cell
362 at $j = 50 \text{ mA cm}^{-2}$ [21]. SPEF with BDD anode at low j is then very effective and
363 extraordinarily efficient, being particularly well suited for treatments in real water matrices.

364 3.3. SPEF treatment in real wastewater matrix using a RuO₂-based/air-diffusion cell

365 Once verified the very good results applying SPEF with BDD, the interest was to replace
366 this anode by a less expensive RuO₂-based anode so as to assess if the system could maintain
367 an acceptable performance.

368 First, the ability of the RuO₂-based/air-diffusion cell to electrogenerate H₂O₂ and active
369 chlorine on site was tested during the SPEF treatment of 2.5 L of a mixture of 0.30 mM MeP
370 + 0.30 mM EtP + 0.30 mM PrP in RWW with 0.20 mM Fe²⁺ at pH 3.0 and $j = 10 \text{ mA cm}^{-2}$,
371 yielding the concentrations depicted in Fig. S5 of Supplementary Material. The H₂O₂ content
372 increased up to a steady concentration of 3.5 mM already reached at 90-120 min. Note the
373 larger value obtained as compared to that with the BDD/air-diffusion cell (Fig. 1), which can

374 be justified by the lower destruction of H₂O₂ at the RuO₂-based surface. On the other hand,
375 active chlorine was accumulated up to 1.3 mg L⁻¹, a similar quantity to that observed with the
376 other cell, which allows concluding that the role of this oxidant during the treatment of
377 parabens with the metal oxide anode is also of minor importance under the present conditions.

378 Fig. 5a shows the concentration abatement of each paraben by SPEF in SWM with 0.20
379 mM Fe²⁺ at pH 3.0 and $j = 10 \text{ mA cm}^{-2}$. Almost total decay (> 95%) was attained after 240
380 min, with no substantial difference among the three profiles, which confirms the prevailing
381 role of •OH formed from Fenton's Reaction (3). From the good fittings considering a pseudo-
382 first-order kinetic analysis shown in the inset, a mean $k = 0.011 \text{ min}^{-1}$ was determined (Table
383 1). In RWW, Fig. 5b highlights that a shorter time of 180 min was needed for attaining > 95%
384 removal by applying SPEF with 0.20 mM Fe²⁺. Again, a unique $k \sim 0.018 \text{ min}^{-1}$ (Table 1) was
385 obtained for the three molecules, which were destroyed faster compared to SPEF in SWM
386 owing to the aforementioned key influence of sunlight irradiation. It can be inferred that, in
387 both media, SPEF with the RuO₂-based anode was slower than using BDD (Fig. 2). This
388 allows concluding that the contribution of M(•OH) cannot be completely disregarded at low j ,
389 in contrast to previous findings in SPEF at high j where the oxidation power of SPEF was
390 independent of the anode nature, as in the case of salicylic acid [54]. For comparison, trials in
391 5 mM Na₂SO₄ were also carried out (Table 1), yielding similar results to those commented in
392 SWM as occurred with the BDD/air-diffusion cell.

393 The effect of Fe²⁺ concentration is also investigated in Fig. 5b. The use of 0.50 mM Fe²⁺
394 led to a substantially quicker disappearance of all parabens until 90 min, which can be
395 accounted for by the acceleration of Fenton's Reaction (3) producing larger quantities of •OH.
396 However, an almost analogous decay was finally attained at 180 min, thus yielding $k = 0.020$
397 min^{-1} (Table 1) that was similar to that at 0.20 mM Fe²⁺. This was due to the complexation of
398 iron ions, which required some time to be photoreduced to free Fe²⁺.

399 Normalized TOC abatements with electrolysis time for the same trials of Fig. 5 are shown
400 in Fig. 6a. In SWM, 35% mineralization was achieved after 240 min. A quite faster TOC
401 decay can be observed during all the electrolysis in RWW with 0.20 mM Fe²⁺, reaching 47%.
402 This agrees with the superiority of SPEF in RWW commented in Fig. 5. If compared with
403 Fig. 3, showing 52% and 66% mineralization in SWM and RWW, respectively, it is evident
404 that the RuO₂-based/air-diffusion cell exhibited a lower oxidation power, reinforcing the idea
405 that the oxidizing role of M([•]OH) cannot be disregarded. Worth mentioning, the progressive
406 deceleration of TOC removal along the treatment, which is partly due to formation of more
407 recalcitrant by-products, precludes a significant accumulation of chloroderivatives, as
408 deduced from the poor production of active chlorine (Fig. S5). Fig. 6a also shows that the
409 addition of a higher amount of Fe²⁺ catalyst (0.50 mM) to perform SPEF in RWW clearly
410 upgraded the treatment at the beginning, thanks to the faster production of hydroxyl radicals.
411 However, the enhancement at 240 min (final mineralization of 52%) was so little that the 0.20
412 mM Fe²⁺ can be considered as optimal. The MCE and EC_{TOC} profiles from all these TOC
413 analyses are gathered in Fig. 6b and c, respectively. A constant MCE of 100% was
414 determined in SWM during the whole electrolysis. Much more efficient treatments were
415 obtained in RWW, starting at about 425% and decaying down to 142% after 240 min. SPEF
416 with 0.50 mM Fe²⁺ was slightly more efficient, attaining 675% as maximum. In
417 correspondence with these trends, the EC_{TOC} values were greater in SWM, being near 95 kWh
418 (kg TOC)⁻¹ versus only 11 kWh (kg TOC)⁻¹ in RWW for 35% TOC reduction. From
419 comparison with the BDD/air-diffusion cell (Fig. 4c), it can be observed that much lower
420 energy was consumed with the RuO₂-based anode, due to the remarkably lower *E*_{cell} (Table
421 S1).

422 Although a relatively high concentration of parabens has been employed in all the above
423 assays, aiming at providing an accurate assessment of the degradation ability of SPEF

424 treatment, it is interesting to evaluate the performance of this technology to remove more
425 realistic contents. The effect of parabens concentration is shown in Fig. 7a for the SPEF
426 degradation of an equimolar mixture (30 μM each) in RWW with 0.20 mM Fe^{2+} at pH 3.0 and
427 $j = 10 \text{ mA cm}^{-2}$. At 180 min, the removal was > 95% for MeP, 88% for EtP and 60% for PrP.
428 The much slower abatement compared to previous trials at 0.30 mM of each paraben can be
429 explained by the greater mass transport limitations inherent to low concentrations of organics,
430 whose reactive events with oxidants become substantially limited. Under these conditions, the
431 treatment is less efficient because $\text{M}(\bullet\text{OH})$ and $\bullet\text{OH}$ are largely consumed in parasitic
432 reactions. Fig. 7b reveals that even at such low content of pollutants, the decays agreed well
433 with a pseudo-first-order kinetics, yielding $k_{\text{MeP}} = 0.016 \text{ min}^{-1} > k_{\text{EtP}} = 0.013 \text{ min}^{-1} > k_{\text{PrP}} =$
434 $5.6 \times 10^{-3} \text{ min}^{-1}$. Hence, in this case the length of the side chain of each paraben had influence
435 on reactivity, which can be justified by the gradually lower diffusion rate to meet the $\text{M}(\bullet\text{OH})$
436 and $\bullet\text{OH}$.

437 For the final optimization of the SPEF treatment of parabens mixtures in RWW with 0.20
438 mM Fe^{2+} at pH 3.0, the influence of applied j was studied within the range 5-30 mA cm^{-2} .
439 From Table 1, it is evident that the pseudo-first-order rate constant for MeP, EtP and PrP
440 gradually increased as j was raised, as expected from the faster production of H_2O_2 that ended
441 in a greater amount of $\bullet\text{OH}$ from Fenton's Reaction (3) as well as from the quicker generation
442 of $\text{M}(\bullet\text{OH})$ from Reaction (1). Thanks to the promotion of larger quantities of oxidants, an
443 analogous upgrade with increasing j was observed for normalized TOC removal ($\text{TOC}_0 = 110$
444 mg L^{-1}) in Fig. 8a, attaining 10%, 47%, 51% and 59% mineralization at 5, 10, 20 and 30 mA
445 cm^{-2} , respectively. In order to evaluate the convenience of using a high j , the corresponding
446 MCE profiles were determined. As shown in Fig. 8b, the efficiency was always lower than
447 100% at 5 mA cm^{-2} , thus giving rise to the less powerful and less efficient SPEF treatment
448 owing to the poor generation of $\text{M}(\bullet\text{OH})$ and $\bullet\text{OH}$. A quite higher MCE was found at 10 mA

449 cm⁻², as commented above. This j became optimal in terms of efficiency, since at 20 and 30
450 mA cm⁻² the maximum MCE value was around 250%, further decreasing down to 100% at
451 240 min. In conclusion, the slightly larger percentage of mineralization at $j > 10$ mA cm⁻² did
452 not counterbalance the much lower efficiency and hence, the higher electrical cost.

453 3.4. Reaction pathways upon SPEF treatment at low input current

454 Four main primary intermediates were detected by GC-MS during the SPEF degradation
455 of a mixture of the three parabens in 5 mM Na₂SO₄ or RWW, always with 0.20 mM Fe²⁺ at
456 pH 3.0, using a BDD/air-diffusion cell at constant j values. The results were verified
457 employing a RuO₂-based/air-diffusion cell.

458 Depending on the sampling time, residual amounts of MeP (m/z 152), EtP (m/z 166) and
459 PrP (m/z 180) could be found at 23.8, 24.1 and 26.2 min, respectively. In Na₂SO₄ medium,
460 three by-products were identified: *p*-hydroxybenzoic acid (m/z 138) at 14.2 min, formed upon
461 hydroxylation of each paraben on the carbonyl group; 3,4-dihydroxy ethylbenzoate (m/z 182)
462 at 30.4 min, which may appear under the attack of M([•]OH) and [•]OH over the aromatic ring of
463 EtP and could be subsequently transformed into *p*-hydroxybenzoic acid; and 3,4-
464 dihydroxybenzoic acid (m/z 154) at 32.4 min, resulting from the additional hydroxylation of
465 the benzenic ring of *p*-hydroxybenzoic acid. In RWW, the additional formation of an
466 organochlorinated by-product, namely 2,4,6-trichlorobenzoic acid (m/z 224) at 30.8 min, was
467 observed. This means that, despite the minor role attributed to active chlorine during the
468 degradation of parabens at low j , its electrogeneration (Fig. 1 and S5) was able to cause the
469 chlorination of the benzenic ring during the attack of hydroxyl radicals. In non-chlorinated
470 media, hydroxylation of the parent paraben on the benzenic ring was also demonstrated upon
471 application of solar photocatalysis with TiO₂ to MeP [44] and EO with BDD to EtP [47]. In
472 our previous study on EF and PEF treatment of MeP, the formation of *p*-hydroxybenzoic acid

473 was shown [48]. On the other hand, different chlorinated parabens were identified in
474 electrochemical [48] and non-electrochemical [47] treatments.

475 To end, the ability of SPEF with the RuO₂/air-diffusion cell at 10 mA cm⁻² to effectively
476 mineralize parabens and their primary by-products was assessed by means of prolonged
477 electrolyses. Fig. S6a of Supplementary Material depicts the TOC decay with electrolysis
478 time for a SPEF trial made in two consecutive days, so as to reach 480 min under a constant
479 natural UV irradiation from sunlight. As much as 70% TOC removal was achieved, a much
480 greater value than 47% attained at 240 min (Fig. 6a). This means that overall mineralization
481 would be feasible at long time using the RuO₂-based anode. The evolution of major linear-
482 chain carboxylic acids formed during this trial can be seen in Fig. S6b of Supplementary
483 Material. Up to 60 and 38 mg L⁻¹ of malic and formic acid were accumulated, respectively, at
484 180-240 min, whereupon a gradual decay to very low values occurred in accordance with
485 TOC abatement promoted by photodecarboxylation via Reaction (10). At 480 min, the
486 residual TOC was probably due to other unidentified aliphatic by-products.

487 **4. Conclusions**

488 This work demonstrates that it is possible to completely decontaminate real wastewater
489 from urban WWTFs containing mixtures of parabens by means of SPEF process with a cheap
490 metal oxide anode. Even more relevant, this has been achieved at low $j = 10 \text{ mA cm}^{-2}$ upon
491 addition of a small amount of Fe²⁺ as catalyst, thus resulting in extraordinarily high
492 efficiencies up to 425% and low energy consumptions. SPEF with BDD anode performed
493 even better, reaching 1000% of MCE but consuming much more energy owing to the higher
494 cell voltage. As a very positive feature, the degradation was always faster in the order Na₂SO₄
495 ~ SWM < RWW, thanks to the high UV power from natural sunlight that regenerates Fe²⁺ via
496 efficient photoreduction of Fe(III) complexes formed with natural organic load. A $j = 10 \text{ mA}$

497 cm⁻² was optimum since a lower or higher current density enhanced the parasitic reactions
498 that wasted the M([•]OH) and [•]OH. Very low concentrations of parabens could also be
499 degraded, although the treatment was decelerated owing to the mass transport limitations. The
500 rate constant decreased in the order $k_{MeP} > k_{EtP} > k_{PrP}$ because the longer side chain gradually
501 caused a slower diffusion. The main reaction pathways involved the hydroxylation on the
502 carbonyl group or the aromatic ring, although one chloroderivative was also identified despite
503 the minor role of electrogenerated active chlorine.

504 **Acknowledgments**

505 Financial support from project CTQ2016-78616-R (AEI/FEDER, EU) is acknowledged.
506 J. R. Steter thanks funding from process number 234142/2014-6 (CNPq, Brazil).

507 **References**

- 508 [1] I. Sirés, E. Brillas, M.A. Oturan, M.A. Rodrigo, M. Panizza, *Environ. Sci. Pollut. Res.*
509 21 (2014) 8336-8367.
- 510 [2] M.A. Oturan, J.-J. Aaron, *Crit. Rev. Environ. Sci. Technol.* 44 (2014) 2577-2641.
- 511 [3] X. Yu, M. Zhou, Y. Hu, K. Groenen Serrano, F. Yu, *Environ. Sci. Pollut. Res.* 21
512 (2014) 8417-8431.
- 513 [4] W. Wu, Z.-H. Huang, T.-T. Lim, *Appl. Catal. A: Gen.* 480 (2014) 58-78.
- 514 [5] C.A. Martínez-Huitle, M.A. Rodrigo, I. Sirés, O. Scialdone, *Chem. Rev.* 115 (2015)
515 13362-13407.
- 516 [6] A. Dirany, I. Sirés, N. Oturan, A. Özcan, M.A. Oturan, *Environ. Sci. Technol.* 46
517 (2012) 4074-4082.
- 518 [7] S. Cotillas, J. Llanos, M.A. Rodrigo, P. Cañizares, *Appl. Catal. B: Environ.* 162 (2015)
519 252-259.

- 520 [8] J. Paramo-Vargas, A. Mounserrath Estrada Camargo, S. Gutierrez-Granados, L.A.
521 Godinez, J.M. Peralta-Hernandez, J. *Electroanal. Chem.* 754 (2015) 80-86.
- 522 [9] K.V. Plakas, S.D. Sklari, D.A. Yiankakis, G.Th. Sideropoulos, V.T. Zaspalis, A.J.
523 Karabelas, *Water Res.* 91 (2016) 183-194.
- 524 [10] L. Liang, F. Yu, Y. An, M. Liu, M. Zhou, *Environ. Sci. Pollut. Res.* 24 (2017) 1122-
525 1132.
- 526 [11] S. Randazzo, O. Scialdone, E. Brillas, I. Sirés, *J. Hazard. Mater.* 192 (2011) 1555-1564.
- 527 [12] A. Da Pozzo, E. Petrucci, *Desalin. Water Treat.* 53 (2015) 1352-1360.
- 528 [13] T. Liu, K. Wang, S. Song, A. Brouzgou, P. Tsiakaras, Y. Wang, *Electrochim. Acta* 194
529 (2016) 228-238.
- 530 [14] H. Roth, Y. Gendel, P. Buzatu, O. David, M. Wessling, *J. Hazard. Mater.* 307 (2016) 1-
531 6.
- 532 [15] S. Lanzalaco, I. Sirés, M.A. Sabatino, C. Dispenza, O. Scialdone, A. Galia,
533 *Electrochim. Acta* 246 (2017) 812-822.
- 534 [16] C. Salazar, C. Ridruejo, E. Brillas, J. Yáñez, H.D. Mansilla, I. Sirés, *Appl. Catal. B:*
535 *Environ.* 203 (2017) 189-198.
- 536 [17] W. Wei, Y. Lu, H. Luo, G. Liu, R. Zhang, *RSC Adv.* 7 (2017) 25627-25633.
- 537 [18] C. Lizama-Bahena, A. Álvarez-Gallegos, J.A. Hernandez, S. Silva-Martinez, *Desalin.*
538 *Water Treat.* 55 (2015) 3683-3693.
- 539 [19] S. Ellouze, S. Kessemtni, D. Clematis, G. Cerisola, M. Panizza, S. Chaâbane Elaoud, J.
540 *Electroanal. Chem.* 799 (2017) 34-39.
- 541 [20] A. Cruz-Rizo, S. Gutiérrez-Granados, R. Salazar, J.M. Peralta-Hernández, *Sep. Purif.*
542 *Technol.* 172 (2017) 296-302.
- 543 [21] F. Gozzi, I. Sirés, A. Thiam, S.C. de Oliveira, A. Machulek Jr., E. Brillas, *Chem. Eng. J.*
544 310 (2017) 503-513.

- 545 [22] R. Salazar, E. Brillas, I. Sirés, *Appl. Catal. B: Environ.* 115-116 (2012) 107-116.
- 546 [23] A. Thiam, I. Sirés, E. Brillas, *Water Res.* 81 (2015) 178-187.
- 547 [24] A. Thiam, I. Sirés, F. Centellas, P.L. Cabot, E. Brillas, *Chemosphere* 136 (2015) 1-8.
- 548 [25] C. Espinoza, J. Romero, L. Villegas, L. Cornejo-Ponce, R. Salazar, *J. Hazard. Mater.*
549 319 (2016) 24-33.
- 550 [26] H. Olvera-Vargas, N. Oturan, M.A. Oturan, E. Brillas, *Sep. Purif. Technol.* 146 (2015)
551 127-135.
- 552 [27] T. Pérez, I. Sirés, E. Brillas, J.L. Nava, *Electrochim. Acta* 228 (2017) 45-56.
- 553 [28] N. Flores, I. Sirés, J.A. Garrido, F. Centellas, R.M. Rodríguez, P.L. Cabot, E. Brillas, *J.*
554 *Hazard. Mater.* 319 (2016) 3-12.
- 555 [29] F.C. Moreira, J. Soler, A. Fonseca, I. Saraiva, R.A.R. Boaventura, E. Brillas, V.J.P.
556 Vilar, *Appl. Catal. B: Environ.* 182 (2016) 161-171.
- 557 [30] A. Thiam, E. Brillas, F. Centellas, P.L. Cabot, I. Sirés, *Electrochim. Acta* 173 (2015)
558 523-533.
- 559 [31] G. Coria, I. Sirés, E. Brillas, J.L. Nava, *Chem. Eng. J.* 304 (2016) 817-825.
- 560 [32] Z.G. Aguilar, E. Brillas, M. Salazar, J.L. Nava, I. Sirés, *Appl. Catal. B: Environ.* 206
561 (2017) 44-52.
- 562 [33] J. Boberg, C. Taxvig, S. Christiansen, U. Hauss, *Reprod. Toxicol.* 30 (2010) 301-312.
- 563 [34] P.W. Harvey, D.J. Everett, *J. Appl. Toxicol.* 24 (2004) 1-4.
- 564 [35] B.A.F. Hafeez, M.D.H. Maibach, *Skin Therapy Lett.* 18 (2013) 5-6.
- 565 [36] F.A. Andersen, *Int. J. Toxicol.* 27 (2008) 1-82.
- 566 [37] Y. Guo, K. Kannan, *Environ. Sci. Technol.* 47 (2013) 14442-14449.
- 567 [38] C. Haman, X. Dauchy, C. Rosin, J.-F. Munoz, *Water Res.* 68 (2015) 1-11.
- 568 [39] W. Li, Y. Shi, L. Gao, J. Liu, Y. Cai, *J. Hazard. Mater.* 300 (2015) 29-38.

- 569 [40] E.M. Cuerda-Correa, J.R. Domínguez, M.J. Muñoz-Peña, T. González, *Ind. Eng. Chem.*
570 *Res.* 55 (2016) 5161-5172.
- 571 [41] R.C. Martins, M. Gmurek, A.F. Rossi, V. Corceiro, R. Costa, M.E. Quinta-Ferreira, S.
572 Ledakowicz, R.M. Quinta-Ferreira, *Water Sci. Technol.* 74 (2016) 1867-1875.
- 573 [42] H. Zúñiga-Benítez, C. Aristizábal-Ciro, G.A. Peñuela, *J. Taiwan Inst. Chem. Technol.*
574 59 (2016) 380-388.
- 575 [43] H. Fang, Y. Gao, G. Li, J. An, P.-K. Wong, H. Fu, S. Yao, X. Nie, *T. An, Environ. Sci.*
576 *Technol.* 47 (2013) 2704-2712.
- 577 [44] T. Velegraki, E. Hapeshi, D. Fatta-Kassinos, I. Poulios, *Appl. Catal. B: Environ.* 178
578 (2015) 2-11.
- 579 [45] J.R. Steter, D. Dionisio, M.R.V. Lanza, A.J. Motheo, *J. Appl. Electrochem.* 44 (2014)
580 1317-1325.
- 581 [46] J.R. Steter, R.S. Rocha, D. Dionisio, M.R.V. Lanza, A.J. Motheo, *Electrochim. Acta*
582 117 (2014) 127-133.
- 583 [47] Z. Frontistis, M. Antonopoulou, M. Yazirdagi, Z. Kilinic, I. Konstantinou, A.
584 Katsaounis, D. Mantzavinos, *J. Environ. Manage.* 195 (2017) 148-156.
- 585 [48] J.R. Steter, E. Brillas, I. Sirés, *Electrochim. Acta* 222 (2016) 1464-1474.
- 586 [49] F.J. Welcher, *Standard Methods of Chemical Analysis*, 6th Edition, Vol. 2, part B, R.E.
587 Krieger Publishing Co Huntington, New York, 1975.
- 588 [50] APWA, AWWA, WEF, *Standard Methods for the Examination of Water and*
589 *Wastewater*, 21st Ed. Method number 4500-Cl Chlorine (residual)–G. DPD
590 Colorimetric Method, American Public Health Association, Washington D.C., 2005, pp.
591 4-67 to 4-68.
- 592 [51] A. Thiam, I. Sirés, J.A. Garrido, R.M. Rodríguez, E. Brillas, *Sep. Purif. Technol.* 140
593 (2015) 43-52.

- 594 [52] N. Kishimoto, Y. Nakamura, M. Kato, H. Otsu, Chem. Eng. J. 260 (2015) 590-595.
- 595 [53] C. Ridruejo, C. Salazar, P.L. Cabot, F. Centellas, E. Brillas, I. Sirés, Chem. Eng. J. 326
596 (2017) 811-819.
- 597 [54] E. Guinea, C. Arias, P.L. Cabot, J.A. Garrido, R.M. Rodríguez, F. Centellas, E. Brillas,
598 Water Res. 42 (2008) 499-511.
- 599

600 **Figure captions**

601 **Fig. 1.** Time course of the concentration of (○,□) H₂O₂ and (●,■) active chlorine
602 accumulated during the SPEF treatment of 2.5 L of a mixture of methylparaben, ethylparaben
603 and propylparaben (0.30 mM each) in (○,●) simulated water matrix and (□,■) real
604 wastewater, with 0.20 mM Fe²⁺ at pH 3.0, using a pre-pilot flow plant with a BDD/air-
605 diffusion cell of 20 cm² electrode area at current density (*j*) of 10 mA cm⁻² and 30 °C.

606 **Fig. 2.** Concentration decay of (○) methylparaben, (□) ethylparaben and (△) propylparaben
607 with electrolysis time during the degradation of 2.5 L of an equimolar mixture (0.30 mM
608 each) in (a) simulated water matrix and (b) real wastewater, with 0.20 mM Fe²⁺ at pH 3.0, by
609 SPEF using a pre-pilot plant with a BDD/air-diffusion cell at *j* = 10 mA cm⁻² and 30 °C. The
610 inset panels present the corresponding pseudo-first-order kinetic analysis.

611 **Fig. 3.** Normalized TOC removal vs. electrolysis time for the SPEF treatments of Fig. 2 using
612 (●) simulated water matrix and (■) real wastewater.

613 **Fig. 4.** Change of (a) mineralization current efficiency and (b) specific energy consumption
614 per unit TOC mass with electrolysis time for the SPEF treatment of 2.5 L of 0.30 mM
615 methylparaben + 0.30 mM ethylparaben + 0.30 mM propylparaben in (▲) 5 mM Na₂SO₄,
616 (●) simulated water matrix and (■) real wastewater, all with 0.20 mM Fe²⁺ of pH 3.0, using
617 a pre-pilot plant equipped with a BDD/air-diffusion cell at *j* = 10 mA cm⁻² and 30 °C.

618 **Fig. 5.** Concentration abatement of (○,◇) methylparaben, (□,▽) ethylparaben and (△,+)
619 propylparaben vs. electrolysis time for the treatment of 2.5 L of an equimolar mixture (0.30
620 mM each) in (a) simulated water matrix and (b) real wastewater at pH 3.0 by SPEF using a
621 pre-pilot plant with a RuO₂-based/air-diffusion cell at *j* = 10 mA cm⁻² and 30 °C. [Fe²⁺] =
622 (○,□,△) 0.20 mM and (◇,▽,+) 0.50 mM. The pseudo-first-order kinetic analysis is shown
623 in the insets.

624 **Fig. 6.** Time course of (a) normalized TOC, (b) mineralization current efficiency and (c)
625 specific energy consumption per unit TOC mass during the SPEF treatments of Fig. 5. (●)
626 Simulated water matrix with 0.20 mM Fe²⁺, and real wastewater with (■) 0.20 and (◆) 0.50
627 mM Fe²⁺.

628 **Fig. 7.** (a) Variation of the concentration of (○) methylparaben, (□) ethylparaben and (△)
629 propylparaben with electrolysis time for the SPEF degradation of an equimolar mixture (30
630 μM each) in real wastewater with 0.20 mM Fe²⁺ at pH 3.0 using a pre-pilot plant with a
631 RuO₂-based/air-diffusion cell at $j = 10 \text{ mA cm}^{-2}$ and 30 °C. (b) Pseudo-first-order kinetic
632 analysis of concentration decays.

633 **Fig. 8.** (a) Normalized TOC removal and (b) mineralization current efficiency with
634 electrolysis time during the SPEF treatment of 2.5 L of a mixture containing 0.30 mM
635 methylparaben + 0.30 mM ethylparaben + 0.30 mM propylparaben in real wastewater with
636 0.20 mM Fe²⁺ at pH 3.0 and 30 °C using a pre-pilot plant with a RuO₂-based/air-diffusion cell
637 at $j =$ (●) 5 mA cm⁻², (■) 10 mA cm⁻², (◆) 20 mA cm⁻² and (▼) 30 mA cm⁻².

638
639
640
641
642
643
644
645
646
647
648
649
650
651
652
653
654
655
656
657
658
659
660
661
662
663

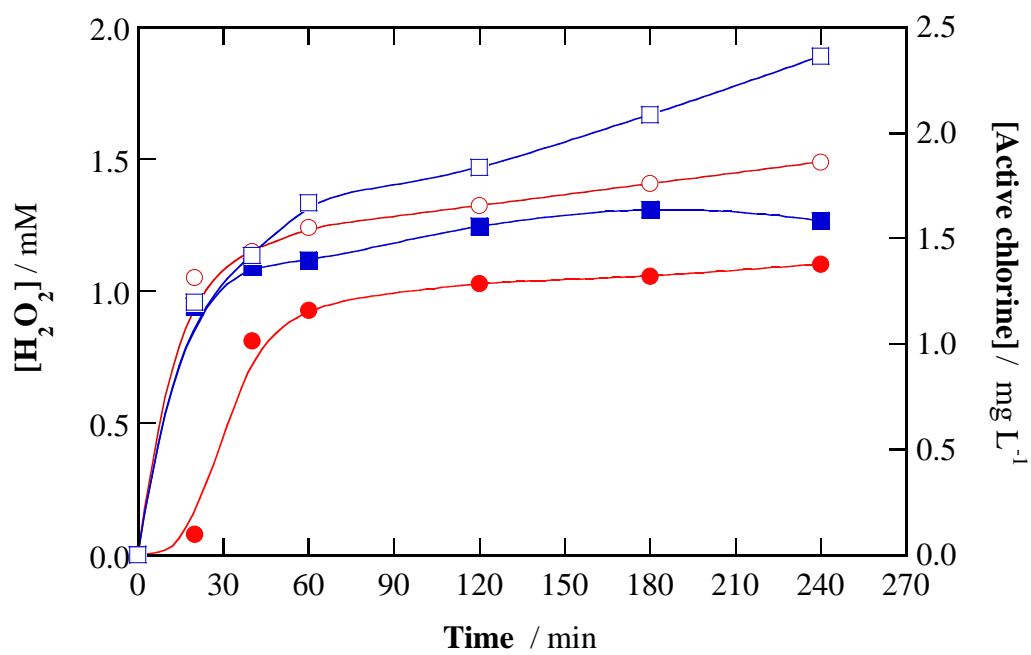


Fig. 1

664
665
666
667
668
669
670
671
672
673
674
675
676
677
678
679
680
681
682
683
684
685
686
687
688
689
690

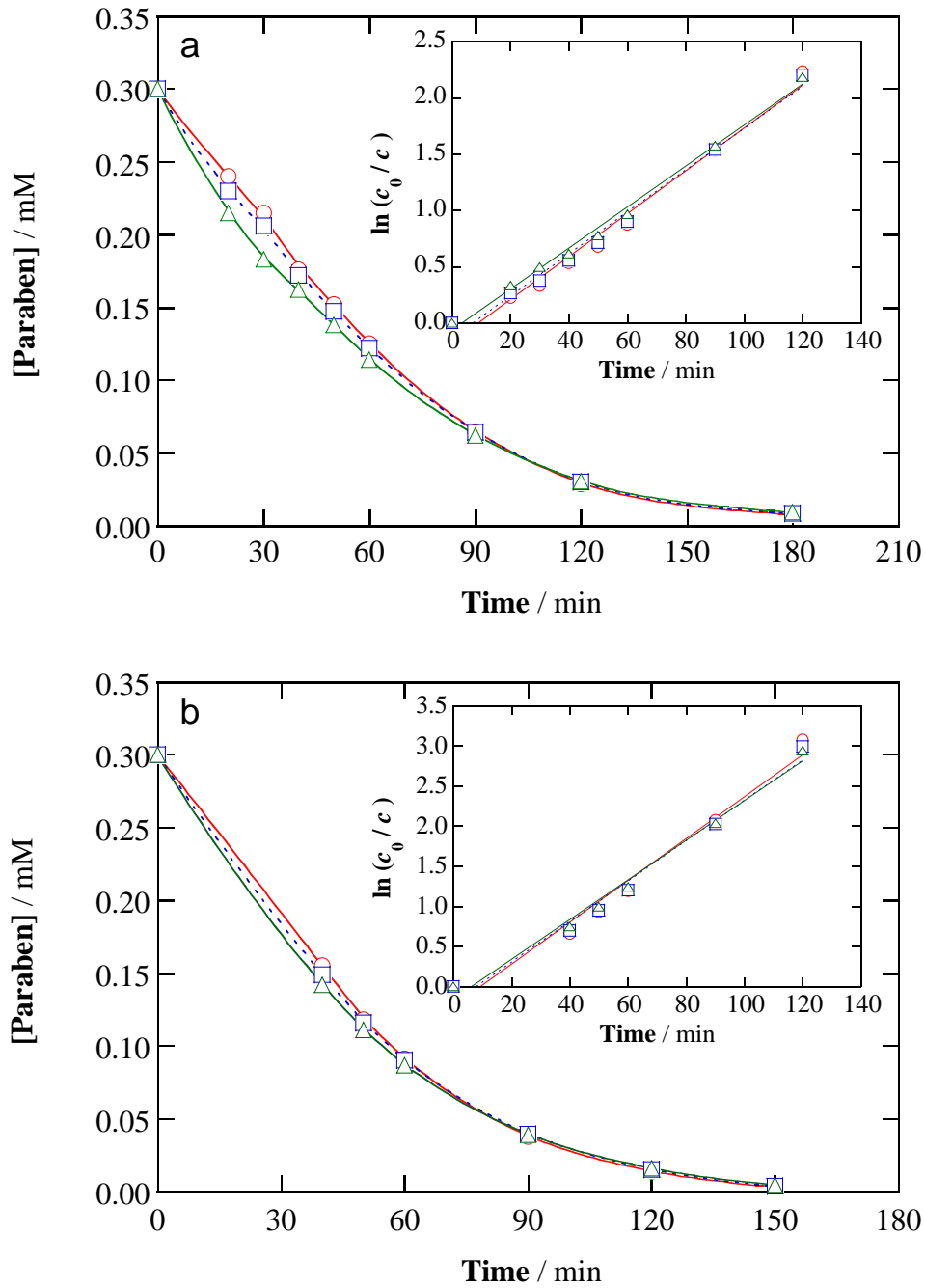


Fig. 2

691

692

693

694

695

696

697

698

699

700

701

702

703

704

705

706

707

708

709

710

711

712

713

714

715

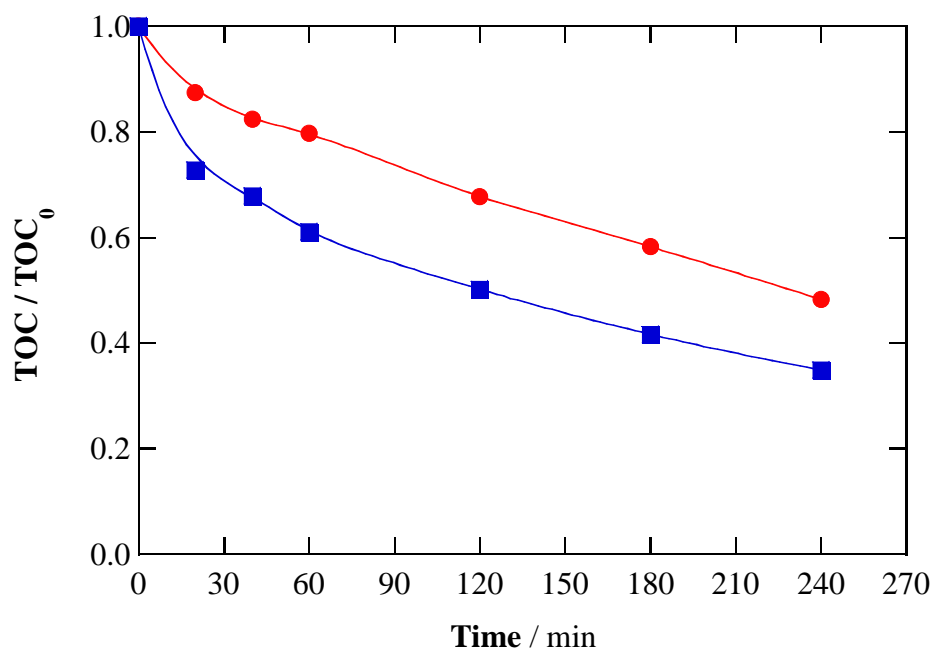


Fig. 3

716
717
718
719
720
721
722
723
724
725
726
727
728
729
730
731
732
733
734
735
736
737
738
739
740
741
742

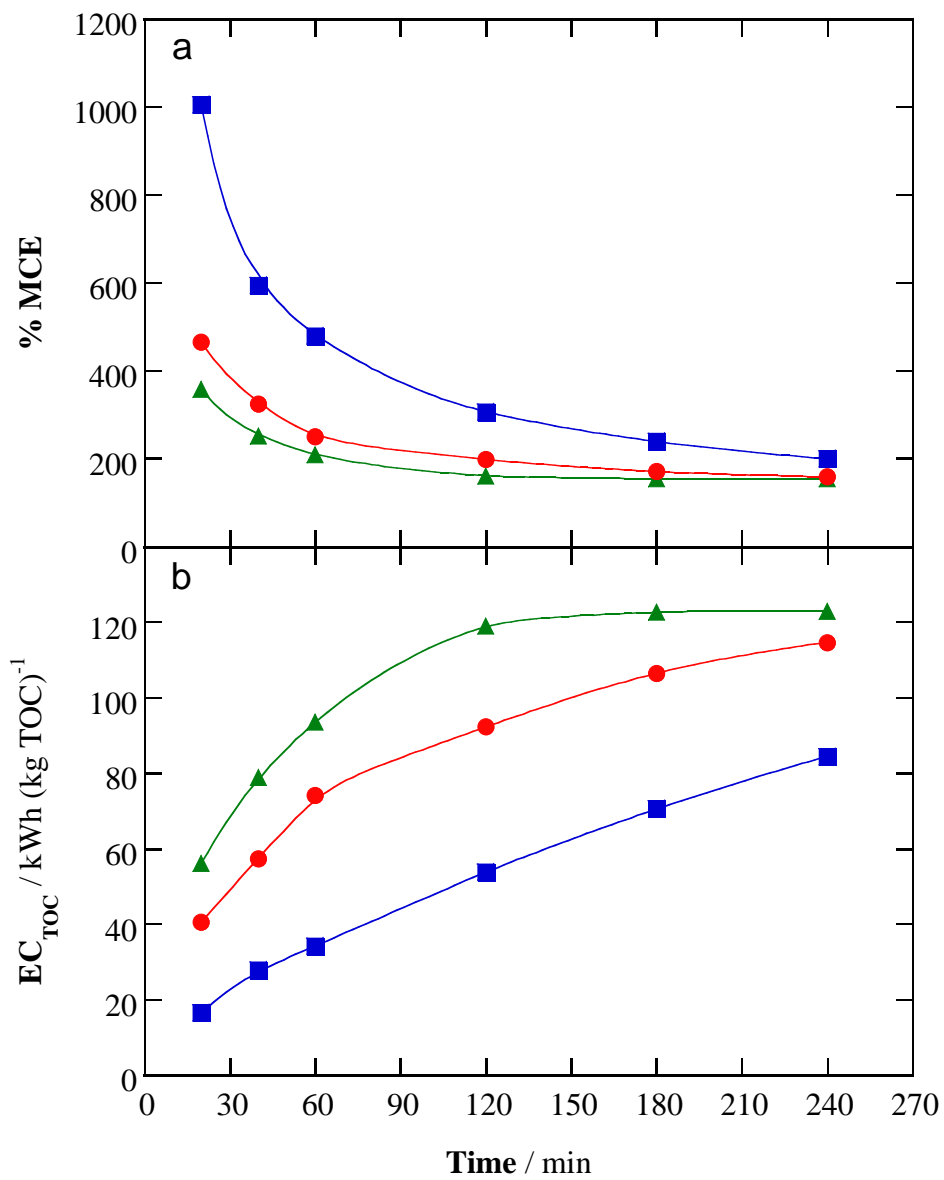


Fig. 4

743
744
745
746
747
748
749
750
751
752
753
754
755
756
757
758
759
760
761
762
763
764
765
766
767

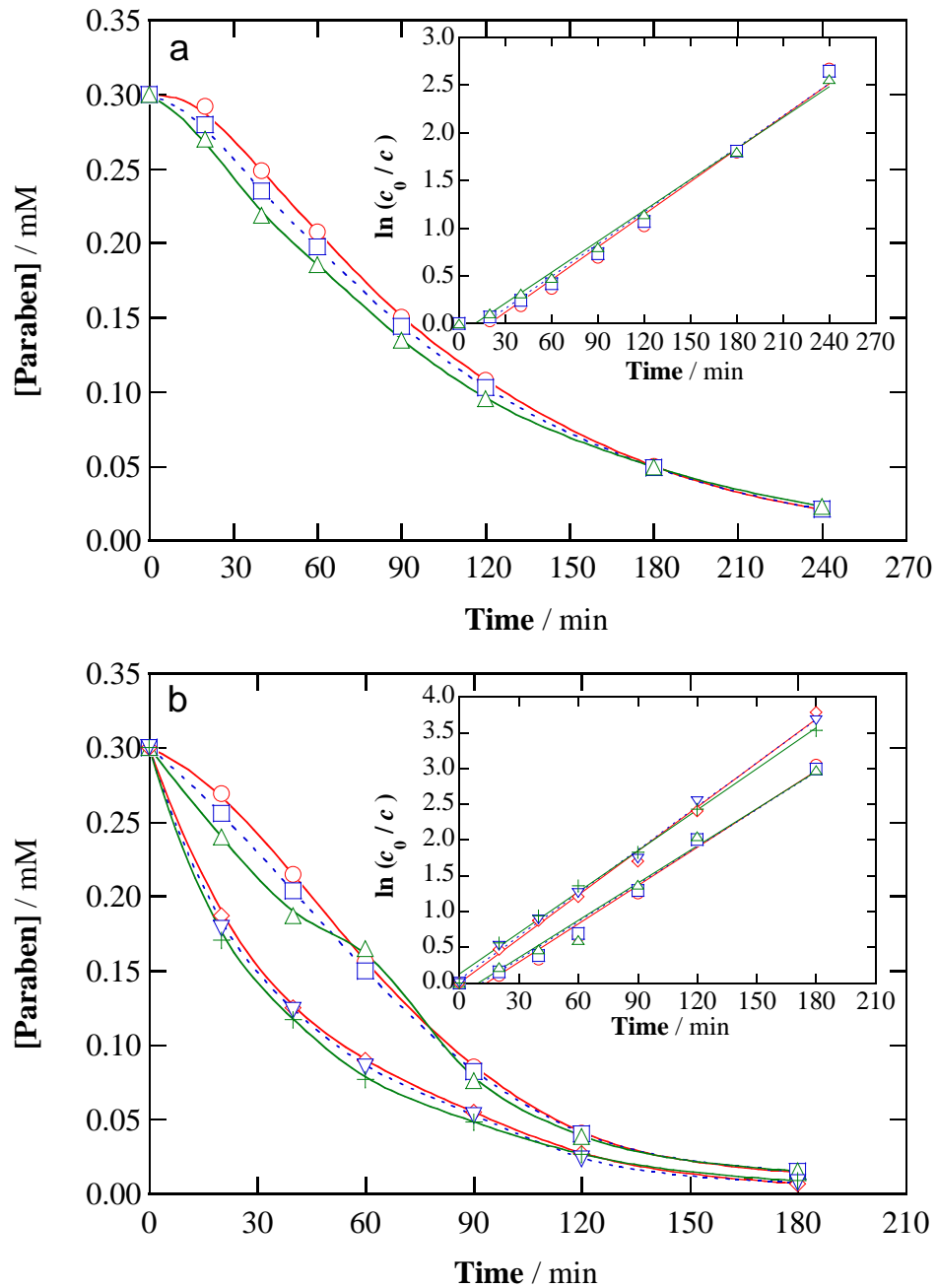


Fig. 5

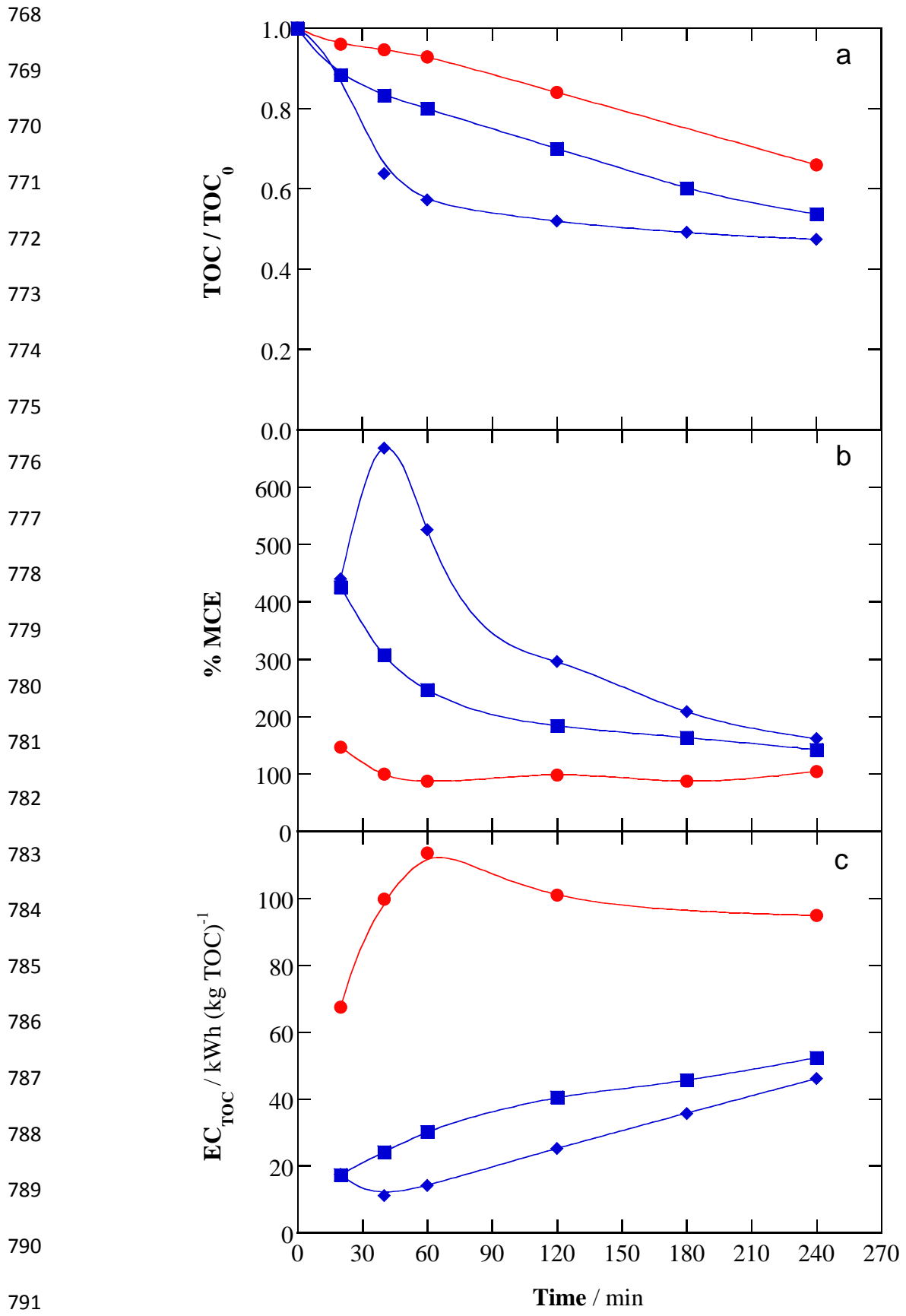


Fig. 6

793

794

795

796

797

798

799

800

801

802

803

804

805

806

807

808

809

810

811

812

813

814

815

816

817

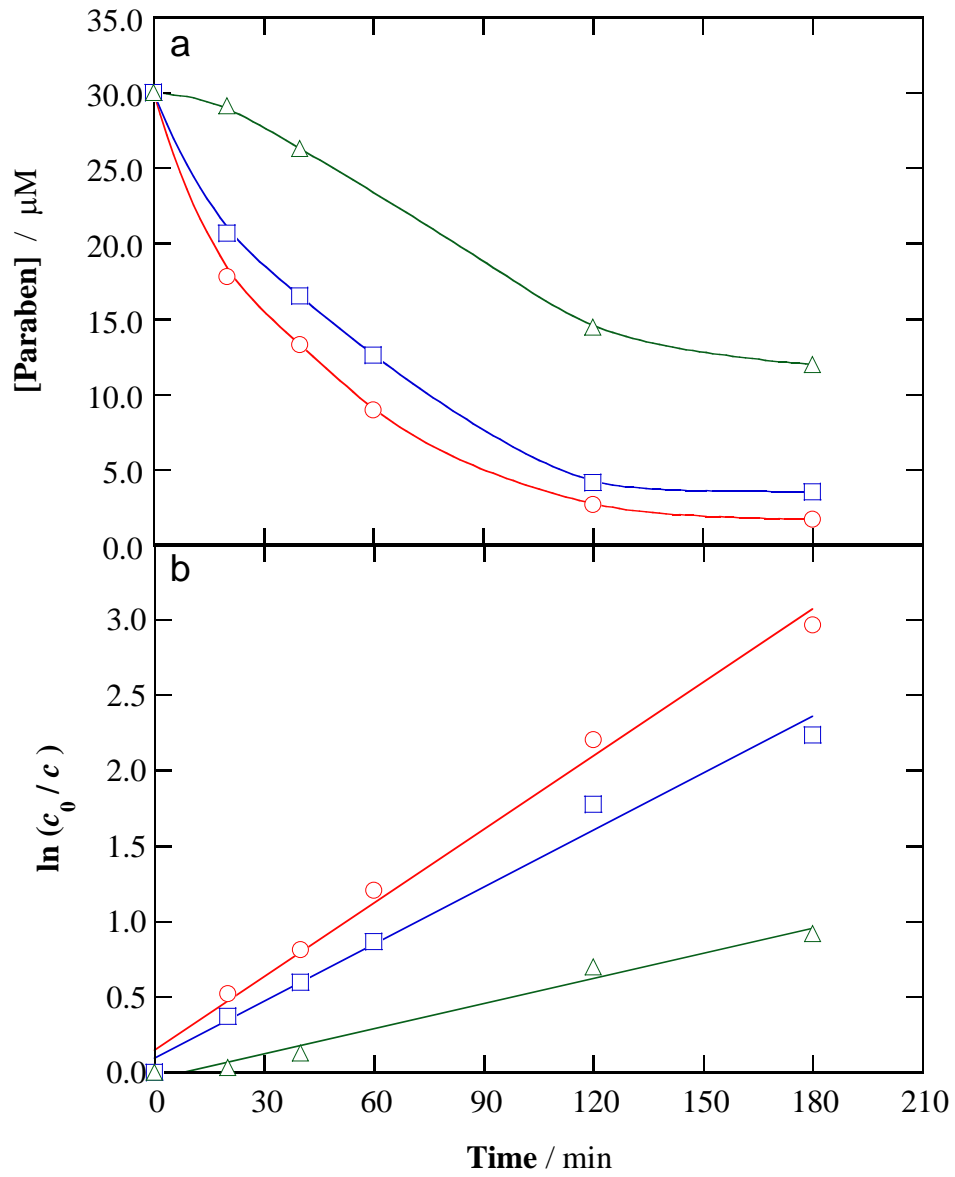


Fig. 7

818
819
820
821
822
823
824
825
826
827
828
829
830
831
832
833
834
835
836
837
838
839
840
841
842

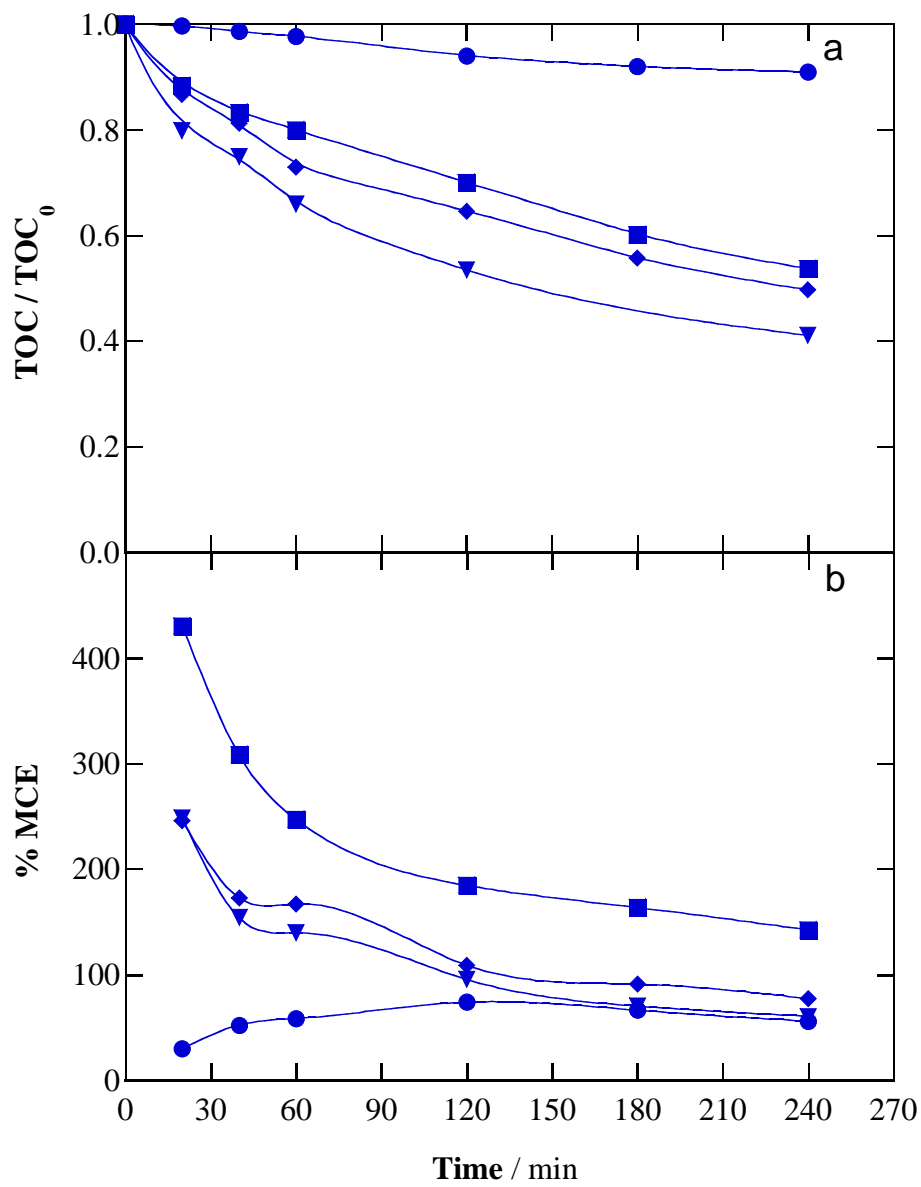


Fig. 8

843 **Table 1**

844 Pseudo-first-order rate constant for methylparaben (k_{MeP}), ethylparaben (k_{EtP}) and
 845 propylparaben (k_{PrP}), along with the corresponding R -squared, obtained upon degradation of 2.5
 846 L of equimolar mixtures (0.30 mM each) in different matrices at pH 3.0 using a pre-pilot plant
 847 containing a cell with an air-diffusion cathode under selected conditions

848

Anode	Process	Medium ^a	j (mA cm ⁻²)	k_{MeP} (min ⁻¹)	R^2	k_{EtP} (min ⁻¹)	R^2	k_{PrP} (min ⁻¹)	R^2
BDD	EO-H ₂ O ₂	5-S	10	2.5×10 ⁻³	0.997	2.6×10 ⁻³	0.995	3.1×10 ⁻³	0.987
	EF ^b	5-S	10	0.013	0.991	0.013	0.994	0.012	0.997
	SPEF ^b	5-S	10	0.021	0.993	0.020	0.996	0.020	0.998
	SPEF ^b	SWM	10	0.019	0.982	0.019	0.987	0.018	0.994
	SPEF ^b	RWW	10	0.026	0.980	0.025	0.980	0.025	0.985
RuO ₂ -based	SPEF ^b	5-S	10	0.014	0.993	0.014	0.992	0.012	0.996
	SPEF ^b	SWM	10	0.011	0.982	0.011	0.988	0.011	0.995
	SPEF ^b	RWW	5	7.2×10 ⁻³	0.984	7.3×10 ⁻³	0.993	7.7×10 ⁻³	0.995
	SPEF ^b	RWW	10	0.018	0.983	0.017	0.987	0.018	0.992
	SPEF ^b	RWW	20	0.025	0.981	0.025	0.983	0.024	0.980
	SPEF ^b	RWW	30	0.031	0.985	0.030	0.987	0.030	0.987
	SPEF ^c	RWW	10	0.020	0.996	0.020	0.997	0.019	0.996

849 ^a 5-S: 5 mM Na₂SO₄; SWM: simulated water matrix; RWW: real wastewater850 ^b 0.20 mM Fe²⁺ added to the solution851 ^c 0.50 mM Fe²⁺ added to the solution